analytical chemistry

pubs.acs.org/ac Article

Monitoring Reaction Intermediates in Plasma-Driven SO_2, NO, and NO_2 Remediation Chemistry Using In Situ SERS Spectroscopy

Shujin Li, Bofan Zhao, Alejo Aguirre, Yu Wang, Ruoxi Li, Sisi Yang, Indu Aravind, Zhi Cai, Ran Chen, Lasse Jensen, and Stephen B. Cronin*

Cite This: https://doi.org/10.1021/acs.analchem.0c05413 Read Online

ACCESS | Metrics & More | Article Recommendations | Supporting Information

ABSTRACT: In situ surface-enhanced Raman scattering (SERS) spectroscopy is used to identify the key reaction intermediates during the plasma-based removal of NO and SO_2 under dry and wet conditions on Ag nanoparticles. Density functional theory (DFT) calculations are used to confirm the experimental observations by calculating the vibrational modes of the surface-bound intermediate species. Here, we provide spectroscopic evidence that the wet plasma increases the SO_2 and the NO_x removal through the formation of highly reactive OH radicals, driving the reactions to H_2SO_4 and HNO_3, respectively. We observed the formation of SO_3 and SO_4 species in the SO_2 wet-plasma-driven remediation, while in the dry plasma, we only identified SO_3 adsorbed on the Ag surface. During the removal of NO in the dry and wet plasma, both NO_2 and NO_3 species were observed on the Ag surface; however, the concentration of NO_3 species was enhanced under wet-plasma conditions. By closing the loop between the experimental and DFT-calculated spectra, we identified not only the adsorbed species associated with each peak in the SERS spectra but also their orientation and adsorption site, providing a detailed atomistic picture of the chemical reaction pathway and surface interaction chemistry.

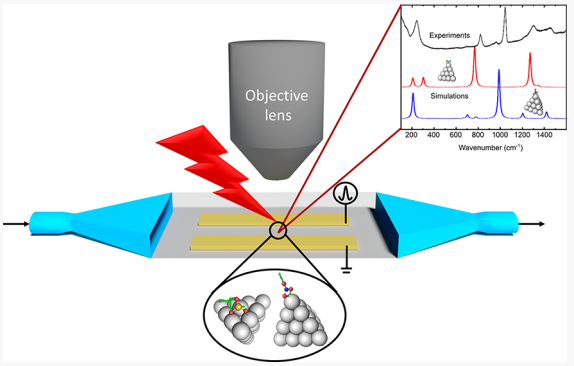

Nitrogen oxide (NO), nitrogen dioxide (NO_2), and sulfur dioxide (SO_2) are toxic by-products of burning fossil fuels. These NO_x emissions are one of the key factors responsible for acid rain and atmospheric photochemical smog. In addition to NO_x regulations, starting January 1, 2020, the International Marine Organization (IMO) has limited the sulfur content in fuel oil used on board ships from 3.5% (i.e., heavy fuel oil) to 0.50% m/m.[1] At this time, heavy fuel oil ("Bunker Fuel") comprises 4% of every barrel of crude oil, which corresponds to 10 000 tons/day of global sulfur emissions. The new 0.5% limit corresponds to a 90% reduction in SO_x emissions, which can potentially be achieved using a plasma-generated OH radical-based approach.[1,2] Although technologies for removing NO_x efficiently currently exist (e.g., selective catalytic reduction (SCR)), effective methods for SO_x treatment are still lacking.[3] For example, the efficiency of SO_x wet scrubber technologies is limited by the low SO_2 solubility in water, which is some orders of magnitude lower than the H_2SO_4 solubility. As such, one attractive solution is to first convert SO_2 to H_2SO_4 (i.e., $SO_2 \rightarrow HSO_3 \rightarrow H_2SO_4$) via the plasma generation of OH radicals and then capture the products by means of a "wet scrubber" with nearly unity capture.[1,3]

In recent years, plasma-based processes have been successfully proven for highly effective NO remediation by many research groups (including our own).[4−18] However, the plasma-based treatment of SO_2 remains challenging. This problem is intensified in diesel exhaust due to the rapid consumption of the vast majority of the oxygen radicals in the plasma by the oxidation of NO to NO_2. In other words, the NO remediation reaction is a competing reaction pathway for the plasma-generated radicals. Yamamoto's group used a single-stage wet-type plasma reactor for the removal of particulates, NO_x, and SO_x simultaneously.[2] More recently, we reported a substantial enhancement in SO_2 removal by discharging a transient nanosecond pulsed plasma in a water vapor-saturated gas mixture.[1] However, the detailed reaction mechanism with the plasma-based process is complex and not fully understood.[19] Figures S1 and S2 of the Supporting Information illustrate the multitude of possible chemical pathways in these plasma-based processes. Here, the major products and intermediates are NO_2, N_2O, N_2O_5, N_2, HNO_2, and HNO_3 for the NO_x removal, while SO_2, SO_3, HSO_3, and H_2SO_4 are present during the SO_xremoval. Nevertheless, identifying the surface intermediate species involved in the

Received: December 25, 2020
Accepted: April 1, 2021

chemical reaction is very difficult using conventional methods for product analysis.

Since its discovery, more than four decades ago, surface-enhanced Raman scattering (SERS) has shown significant promise for sensing individual molecules adsorbed onto metal nanostructures or substrates with nanoscale roughness.[20−24] SERS is a highly sensitive vibrational spectroscopic technique that allows the detection of low concentrations of molecules through the amplification of electromagnetic fields generated by the excitation of surface plasmons. In short, SERS significantly increases the signal from the weak yet structurally rich technique of Raman scattering. Thus, SERS presents a promising technique for the identification of surface active species during the NO_x and SO_x removal processes. However, the SERS spectral signatures are mainly determined by the interactions between molecules and surfaces. Therefore, a correct interpretation of the chemical mechanism in SERS is required to extract the vibrational information contained in these spectra.[25] First-principles calculations enable a consistent treatment of the enhancement mechanisms and thus provide a means for interpreting the SERS spectra.[25,26]

In this work, we provide spectroscopic evidence of the intermediates formed during the NO and SO_2 plasma-based removal on Ag nanoparticles by in situ SERS. Moreover, we verify the identification of surface species using density functional theory (DFT) calculations. To our knowledge, this is the first time that experimentally measured SERS vibrational modes of NO_2, NO_3, SO_3, and SO_4 adsorbed on Ag nanoparticles have been confirmed by atomistic simulations, thus, providing peak assignment (e.g., SO_3 vs SO_4), molecular orientation, and adsorption site.

Here, we utilize a transient pulsed plasma discharge in a glass-slide plasma-based reactor, which consists of two parallel copper electrodes separated by an approximately 5 mm gap (see Figure 1).[27−29] Further details are given in the Supporting Information.

Figure 2a shows SERS spectra collected during plasma discharge (13 kV pulses at 200 Hz) in a flowing SO_2 gas environment (5 sccm, 500 PPM) both with and without water vapor. Under these conditions, we have shown that the SO_2 removal is 6× more effective in wet plasma than in dry plasma (see Figure S3).[1] The SERS spectra shown in Figure 2a exhibit similar features to those reported by Hirokawa et al.[30] and Maeda et al.[31] for SO_3 and SO_4 adsorbed on Ag nanoparticles. Here, we find that the SERS spectra are quite different in the dry plasma (i.e., without water vapor) than in the wet plasma (i.e., with water vapor). In the wet-plasma discharge, prominent sharp peaks are observed at 618 and 928 cm^{-1} corresponding to SO_3 species and at 958 and 1044 cm^{-1} corresponding to SO_4 species.[30,31] Additionally, small peaks are detected at 249, 470, and 821 cm^{-1}. In the dry plasma, small peaks at 190, 971, and 1090 cm^{-1} corresponding to SO_3 are observed.[30,31] The main SO_3 peak around 600 cm^{-1} has a somewhat lower relative intensity than that calculated by DFT, and it is broadened and red shifted to 559 cm^{-1}. Additionally, during the dry-plasma discharge, no SO_4 peaks are observed experimentally. As a control experiment, we also flowed H_2SO_4 vapor across the Ag nanoparticles (without plasma discharge), which exhibited prominent peaks at 243, 624, 967, and 1171 cm^{-1}, as shown in Figure S4 of the Supplementary Information. To properly assign and correlate the measured signals, Table 1 lists the vibrational frequencies observed

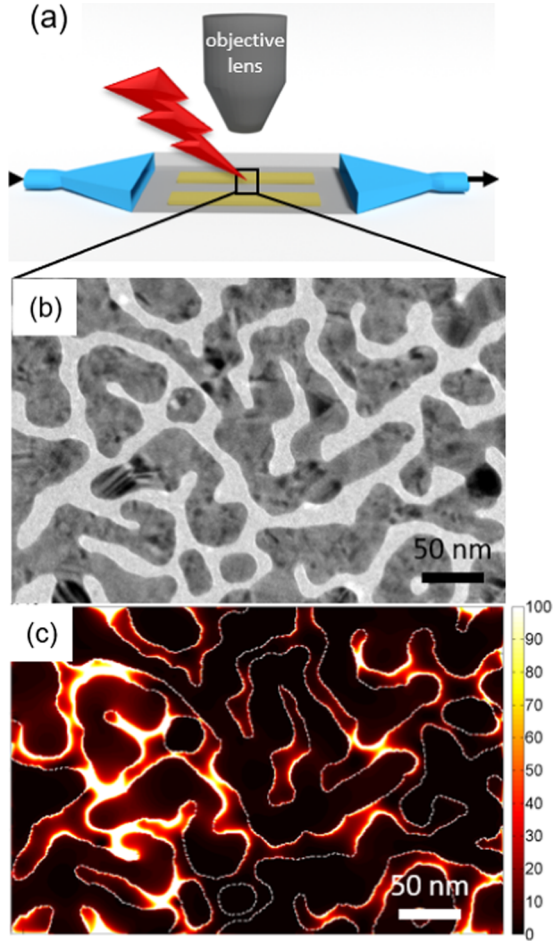

Figure 1. (a) Schematic diagram illustrating our experimental setup consisting of a glass-slide plasma-based reactor with in situ SERS spectroscopy. (b) Transmission electron microscopic (TEM) image of SERS-active Ag nanoislands and (c) the corresponding electron field intensity (E^2) distribution calculated by finite-difference time-domain (FDTD).

during the experiments together with the calculations performed by DFT.

We calculated the adsorption of SO_3 and SO_4 on the Ag nanoparticles by DFT at the Ag atop site and on the (111)Ag surface (see Figures S5 and S6). We found that the SO_3 is adsorbed via the sulfur atom with a binding energy of −5.54 eV for the SO_3 adsorbed to the atop Ag site and −5.33 eV for the SO_3 adsorbed to the (111)Ag surface. SO_4 is bidentate coordinated through two oxygen atoms with an interaction energy of −4.42 eV for the SO_4 adsorbed to the atop Ag site and −4.35 eV for the SO_4 adsorbed to the (111)Ag surface.

Figure 2b,c shows the calculated Raman spectra for SO_3 and SO_4 adsorbed on the Ag clusters. Interestingly, the vibration modes vary significantly for the two Ag surfaces (i.e., atop and (111)). In particular, the dominant features for SO_3 adsorbed to the atop Ag surface site are predicted at 181, 535, and 890 cm^{-1}, corresponding to the S−Ag stretching, O−S bending, and symmetric O−S stretching of sulfite, respectively. For SO_3 adsorbed to (111)Ag surfaces, the main peaks are calculated at 422 cm^{-1} (O−S bending), 449 cm^{-1} (O−S wagging), 551 cm^{-1} (S−Ag stretching + O−S bending), 804 cm^{-1} (symmetric O−S stretching), 864 cm^{-1} (asymmetric O−S stretching), and 1079 cm^{-1} (O−S stretching).

https://doi.org/10.1021/acs.analchem.0c05413
Anal. Chem. XXXX, XXX, XXX−XXX

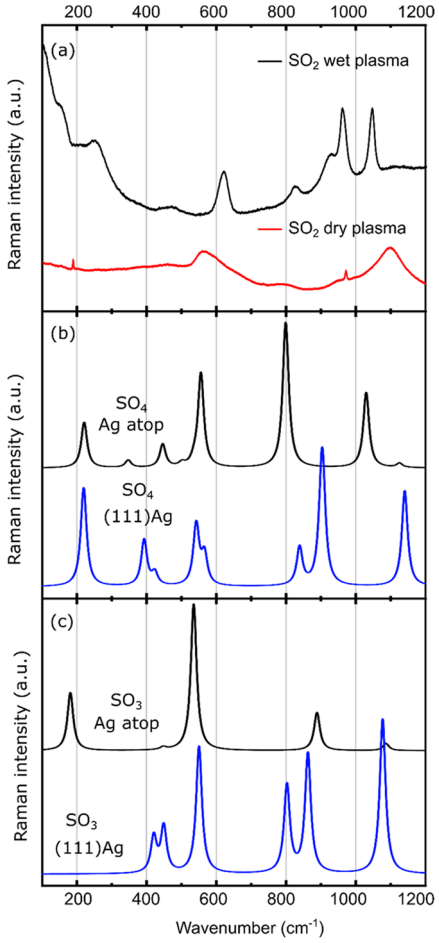

Figure 2. (a) SERS spectra measured during SO_2 removal with dry and wet plasma. SERS spectra of (b) SO_4 and (c) SO_3 species calculated by DFT.

The dominant features for SO_4 adsorbed to the atop Ag surface site are calculated at 221, 446, 556, 799, and 1030 cm^{-1}, corresponding to the S−Ag stretching, O−S bending, S−Ag stretching + O−S bending, symmetric O−S stretching, and symmetric O−S stretching vibrational modes of sulfate, respectively. For SO_4 adsorbed to (111)Ag surfaces, the main Raman signals are predicted at 219 cm^{-1} (relative motion between SO_4 and Ag_{20}), 393 cm^{-1} (O−S waggling), 542 cm^{-1} (O−S bending), 840 cm^{-1} (symmetric O−S stretching), 904 cm^{-1} (asymmetric O−S stretching), and 1141 cm^{-1} (O−S stretching). Detailed drawings of the vibrational modes and frequencies of SO_3 and SO_4 adsorbed on the Ag nanoparticles can be found in Figures S5 and S6 of the Supplementary Information.

During the removal of SO_2 in dry plasma, the small peak observed at 189 cm^{-1} can be assigned to SO_3 adsorbed on a defect site (atop), while the broad peak around 1099 cm^{-1} can be correlated with SO_3 adsorbed on (111)Ag. Additionally, the absence of the peaks around 220, 960, and 1044 cm^{-1} indicates that SO_4 is not present and only SO_3 species are formed. The SO_3 species are present on defect sites during the SO_2 removal reaction in dry-plasma discharge. The spectrum collected during the SO_2 removal with wet plasma shows Raman signals corresponding to SO_3 species adsorbed on the (111)Ag surface at 470 and 821 cm^{-1}. The peak at 1044 cm^{-1} can be assigned to SO_4 adsorbed to the Ag atop site. The peaks at 249, 618,

Table 1. Some Important Vibrational Frequencies of Reactants and Potential Products during SO_2 Plasma Discharge

component	S−Ag stretching	O−S wagging or O−S bending	S−Ag stretching + O−S bending	symmetric O−S stretching	asymmetric O−S stretching + O−S stretching
SO_2 dry-plasma	189 (SO_3)	N/A	559	766 (small)	971/1099
SO_2 wet-plasma	249 (SO_4)	470	618	821	928/958/1044
H_2SO_4	243 (SO_4)	468	624	N/A	1171
SO_3 on Ag atop[a]	181	448 (small)	535	890	1088 (small)
SO_4 on Ag atop[a]	221	446	556	799	1030
SO_3 on (111)Ag[a]	N/A	422/449	551	804	864/1079
SO_4 on (111)Ag[a]	219	393	542	840	904/1141

[a]Values obtained from DFT calculations.

https://doi.org/10.1021/acs.analchem.0c05413
Anal. Chem. XXXX, XXX, XXX−XXX

and 958 cm^{-1} are assigned to SO_4 species. However, for these peaks, it is not possible to discriminate between SO_4 adsorbed on atop or (111)Ag, and probably species on both sites coexist.

The results presented here indicate that SO_2 is partially converted to SO_3 in the dry plasma, with a low SO_2 removal rate. The further oxidation of SO_3 via (HSO_3) is limited, and no SO_4 via H_2SO_4 is detected in the Raman spectra due to low amount of OH radicals. In the wet plasma, the formation of highly reactive OH radicals drives the SO_2 conversion to H_2SO_4 in a two-step process: $SO_2 \rightarrow HSO_3 \rightarrow H_2SO_4$ achieving high SO_2 removal rates. In our previous work, we demonstrated that the wet plasma is 6 times more effective than the dry plasma at removing SO_2.[1] In that previous work, we provided spectroscopic evidence of the short-lived, highly reactive OH radical generation in the presence of vapor water through plasma emission spectroscopy.[1] In the present work, we provide spectroscopic evidence of the SO_4 formation during the removal of SO_2 in the wet plasma. The absence of Raman signals corresponding to adsorbed atop SO_3 in the wet plasma may indicate that this species is rapidly oxidized to SO_4 and, as such, SO_3 and SO_4 species accumulate on the highly coordinated Ag sites.

Figure 3a shows the SERS spectra collected during plasma discharge (13 kV pulses at 200 Hz) in a flowing NO gas environment (5 sccm, 500 ppm) with and without water vapor.

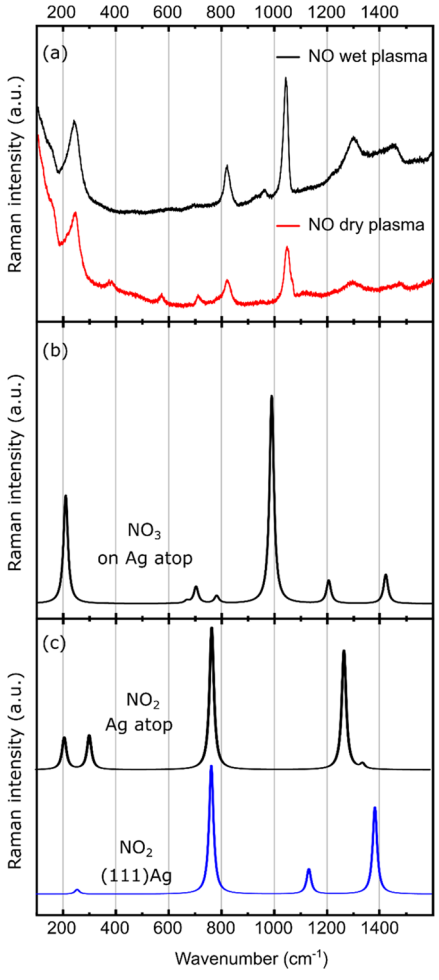

Figure 3. (a) SERS spectra measured during NO removal with dry and wet plasma. SERS spectra of (b) NO_2 and (c) NO_3 species calculated by DFT.

Using a coaxial plasma-based reactor (see Figure S7), we observed NO and NO_x removals of 40 and 4% with dry plasma, respectively, while the wet-plasma discharge produced a removal of 100% for NO and 98% for NO_x.[19] When discharging the dry plasma in NO gas, peaks at 243 and 818 cm^{-1} are observed and assigned to NO_2 species,[32−34] while the peak at 1046 cm^{-1} corresponds to NO_3 species.[33,34] In the wet-plasma discharge, Raman signals are measured at 237, 819, 963, 1041, and 1297/1444 cm^{-1}, showing the formation of NO_2 and NO_3 species.[32−34] The Raman spectra observed during the wet- and dry-plasma discharge cannot be correlated with NO molecules or ions, indicating that NO is adsorbed on the surface as NO_2/NO_3.[33] As a control experiment, we also flowed HNO_3 vapor across Ag nanoparticles (without plasma discharge) (see Figure S8), which showed prominent peaks at 258, 855, 933, 1052, and 1396 cm^{-1}. To further confirm the species observed during the experiments, the spectra are compared with those predicted by DFT calculations. Table 2 lists the vibrational frequencies observed during the experiments together with those predicted by simulations.

We calculated the adsorption of NO_2 and NO_3 on the Ag nanoparticles by DFT at the Ag atop site and on the (111)Ag surface. We found that the NO_2 is adsorbed via the nitrogen atom with a binding energy of −2.14 eV for the NO_2 adsorbed to the atop Ag site and −1.69 eV for the NO_2 adsorbed to the (111)Ag surface. The NO_3 is bidentate coordinated through two oxygen atoms (see Figures S9 and S10) with an interaction energy of −1.68 eV for the NO_3 adsorbed to the atop Ag site, while no stable configuration is found for the NO_3 adsorbed to the (111)Ag surface.

The calculated Raman spectra of NO_2 and NO_3 adsorbed on Ag nanoparticles are plotted in Figure 3b,c. NO_2 adsorbed on the atop Ag surface site exhibits peaks at 207, 303, 769, and 1274 cm^{-1}, corresponding to the N−Ag stretching, N−Ag bending + N−O bending, N−O bending, and N−Ag stretching + N−O bending vibrational modes of nitrite, respectively. For NO_2 adsorbed on the (111)Ag surface, peaks are predicted at 254, 764, and 1135/1387 cm^{-1} and are assigned to the N−Ag bending + N−O bending, N−O bending, and asymmetric N−O stretching of nitrite vibration modes.

The calculated spectrum of NO_3 adsorbed atop on the Ag surface exhibits peaks at 210, 703/781, 989, and 1206/1422 cm^{-1}. The signal at 210 cm^{-1} is assigned to the O−Ag stretching, the signal at 703/781 to the N−O bending, 989 cm^{-1} to symmetric N−O stretching, and the bands at 1206/1422 cm^{-1} to the asymmetric N−O stretching vibrational modes of the surface-bound nitrate species. It is worth mentioning that the DFT calculations could not obtain any stable configuration of the nitrate molecules on the (111)Ag surface. More details of the vibrational modes and frequencies of NO_2 and NO_3 adsorbed on the Ag nanoparticles can be found in Figures S9 and S10.

The spectra observed during the NO removal in dry plasma match nicely with those obtained by DFT for NO_2 adsorbed on the Ag nanoparticles, indicating the formation of nitrites on the surface. Additionally, the absence of the peak around 990 cm^{-1} and the small signal at 1046 cm^{-1} suggests that NO_3 is present on the surface at low concentrations. When the plasma is discharged in a wet NO atmosphere, the Raman signals assigned to NO_3 atop at 963 and 1422 cm^{-1} are clearly seen, together with the signal at 1041 cm^{-1}, which correlates with the reference HNO_3 spectrum. The peaks at 819 and 1297

https://doi.org/10.1021/acs.analchem.0c05413
Anal. Chem. XXXX, XXX, XXX−XXX

Table 2. Some Important Vibrational Frequencies of Reactants and Potential Products during SO_2 Plasma Discharge

component	N–Ag stretching	N–Ag bending + N–O bending	N–O bending	symmetric N–O stretching	asymmetric N–O stretching	N–Ag stretching + N–O bending
NO dry-plasma	243		818	1046	1295	
NO wet-plasma	237		819	963/1041	1297/1444	
HNO_3	258		855	933/1052	1396	N/A
NO_2 on Ag atop[a]	207	303	769	N/A	N/A	1274
NO_3 on Ag atop[a]	210 (O–Ag stretching)	N/A	703/781 (small)	989	1206/1422 (small)	N/A
NO_2 on (111)Ag[a]	N/A	254	764	N/A	1135/1387	N/A
NO_3 on (111)Ag[a]	N/A	N/A	N/A	N/A	N/A	N/A

[a]Values obtained from DFT calculations.

cm^{-1} indicate the presence of NO_2 atop on the Ag surface. This may indicate that the NO_2 and NO_3 species are adsorbed on defect sites during the wet-plasma NO removal.

The results obtained in this work suggest that when discharging the dry plasma in NO gas, it readily converts to NO_2 through atomic oxygen radicals. In the gas phase (i.e., without Ag nanoparticles), the further oxidation to NO_3 is limited by the availability of OH radicals.[18,19] In the presence of Ag nanoparticles, the surface chemistry (i.e., strongly oxidizing nature of Ag) readily converts NO and NO_2 species to NO_3, as evidenced in the Raman spectra with the peak at 1046 cm^{-1}. However, the still low availability of O or OH radicals limits the total conversion to NO_3 (or HNO_3). The presence of water facilitates the formation of OH radicals,[19] enhancing the NO removal by 2.5× and the NO_x removal by 25×, thus improving the HNO_3 (and hence NO_3) production as observed by the in situ SERS spectra. Additionally, the second step minimizes the backreaction of NO_2 to NO. Finally, the HNO_3 can be captured using water and subsequently titrated, with near-unity efficiency in a wet scrubber.

This work demonstrates that the joint SERS/DFT approach can be used to study (and identify) important reaction intermediates, thus, establishing reaction pathways in a complex reaction system. As another practical example, in CO_2 reduction with water, more than a dozen reaction pathways have been proposed. The identification of specific pathways (and their catalytically active sites) can enable new, more selective catalysts to be developed and optimized.

In conclusion, a substantial enhancement in the removal of gaseous NO, NO_2, and SO_2 is reported by discharging a transient nanosecond pulsed plasma in a water vapor-saturated gas mixture compared to dry conditions. We have collected in situ SERS spectra during the plasma-based treatment of toxic gases NO, NO_2, and SO_2 in both dry- and wet-plasma conditions. In addition, we have calculated SERS-enhanced Raman spectra of various intermediate species (including NO_2, NO_3, SO_3, and SO_4) bounded to Ag nanoclusters using density functional theory. The dominant peaks in the simulated spectra qualitatively agree with the experimental spectra and help us to determine the correct assignment of the vibrational modes, adsorbed species, orientation, and adsorption site on the Ag nanoparticles. Through this approach, we were able to identify the reaction intermediates produced during the plasma-driven remediation process. In particular, we observed SO_3 species adsorbed atop and on the (111)Ag surface during the SO_2 removal in dry plasma, while the SO_4 species could not be detected, showing the limitation of the dry-plasma approach to fully convert SO_2 to H_2SO_4. When discharging the wet plasma, both SO_3 and SO_4 species adsorbed on highly coordinated Ag sites were identified. During NO remediation in both dry and wet plasma, NO_2 and NO_3 were detected. However, in the wet-plasma discharge, the SERS results show that the NO_3 production is enhanced. Additionally, we showed that NO_2 and NO_3 species are adsorbed on defect sites during the wet-plasma NO removal. To our knowledge, this is the first time that the active species have been detected by SERS spectroscopy during NO_x and SO_x remediation processes and correlated with theoretical calculations.

https://doi.org/10.1021/acs.analchem.0c05413
Anal. Chem. XXXX, XXX, XXX−XXX

■ ASSOCIATED CONTENT

Supporting Information

The Supporting Information is available free of charge at https://pubs.acs.org/doi/10.1021/acs.analchem.0c05413.

Experimental details; NO and SO_2 removal efficiencies; chemical pathways; reference spectra; and details of the vibrational modes and frequencies of adsorbed molecules on Ag nanoparticles (PDF)

■ AUTHOR INFORMATION

Corresponding Author

Stephen B. Cronin − *Department of Physics and Astronomy, University of Southern California, Los Angeles, California 90089, United States; Ming Hsieh Department of Electrical Engineering, University of Southern California, Los Angeles, California 90089, United States;* orcid.org/0000-0001-9153-7687; Email: scronin@usc.edu

Authors

Shujin Li − *Mork Family Department of Chemical Engineering and Materials Science and Daniel J. Epstein Department of Industrial & System Engineering, University of Southern California, Los Angeles, California 90089, United States*

Bofan Zhao − *Ming Hsieh Department of Electrical Engineering, University of Southern California, Los Angeles, California 90089, United States;* orcid.org/0000-0003-0478-6330

Alejo Aguirre − *Instituto de Desarrollo Tecnológico para la Industria Química (INTEC), Universidad Nacional del Litoral, CONICET, S3000GLN Santa Fe, Argentina*

Yu Wang − *Mork Family Department of Chemical Engineering and Materials Science and Daniel J. Epstein Department of Industrial & System Engineering, University of Southern California, Los Angeles, California 90089, United States;* orcid.org/0000-0002-0307-1301

Ruoxi Li − *Mork Family Department of Chemical Engineering and Materials Science and Daniel J. Epstein Department of Industrial & System Engineering, University of Southern California, Los Angeles, California 90089, United States*

Sisi Yang − *Department of Physics and Astronomy, University of Southern California, Los Angeles, California 90089, United States;* orcid.org/0000-0003-0352-833X

Indu Aravind − *Department of Physics and Astronomy, University of Southern California, Los Angeles, California 90089, United States*

Zhi Cai − *Ming Hsieh Department of Electrical Engineering, University of Southern California, Los Angeles, California 90089, United States*

Ran Chen − *Department of Chemistry, Pennsylvania State University, University Park, Pennsylvania 16802, United States*

Lasse Jensen − *Department of Chemistry, Pennsylvania State University, University Park, Pennsylvania 16802, United States;* orcid.org/0000-0003-1237-5021

Complete contact information is available at: https://pubs.acs.org/10.1021/acs.analchem.0c05413

Author Contributions

The manuscript was written through contributions of all authors. All authors have given approval to the final version of the manuscript.

Notes

The authors declare no competing financial interest.

■ ACKNOWLEDGMENTS

This research was supported by the Army Research Office (ARO) award no. W911NF-19-1-0257 (S.L.); National Science Foundation (NSF) award nos. CHE-1708581 (R.L.), CBET-2012845 (Z.C.), and CBET-1954834 (I.A.); Air Force Office of Scientific Research (AFOSR) grant no. FA9550-19-1-0115 (B.Z.); and U.S. Department of Energy, Office of Basic Energy Sciences award no. DESC0019322 (S.Y.). L.J. and R.C. acknowledge the support from the National Science Foundation Grant CHE-1707657. Portions of this work were conducted with Advanced Cyberinfrastructure computational resources provided by the Institute for Cyber-Science at the Pennsylvania State University (https://ics.psu.edu/).

■ REFERENCES

(1) Schroeder, C.; Schroeder, W.; Yang, S.; Shi, H.; Nystrom, A.; Subramanian, S.; Li, S.; Gundersen, M. A.; Cronin, S. B. *Fuel* **2020**, *274*, No. 117810.

(2) Kuroki, T.; Takahashi, M.; Okubo, M.; Yamamoto, T. *IEEE Trans. Ind. Appl.* **2002**, *38*, 1204−1209.

(3) Brachert, L.; Kochenburger, T.; Schaber, K. *Aerosol Sci. Technol.* **2013**, *47*, 1083−1091.

(4) Namihira, T.; Tsukamoto, S.; Wang, D.; Katsuki, S.; Hackam, R.; Akiyama, H.; Uchida, Y.; Koike, M. *IEEE Trans. Plasma Sci.* **2000**, *28*, 434−442.

(5) Matsumoto, T.; Wang, D.; Namihira, T.; Akiyama, H. *IEEE Trans. Plasma Sci.* **2010**, *38*, 2639−2643.

(6) Matsumoto, T.; Wang, D.; Namihira, T.; Katsuki, S.; Akiyama, H. *Acta Phys. Pol., A* **2009**, *115*, 1101−1103.

(7) Wang, T.; Sun, B.-M.; Xiao, H.-P.; Zeng, J.-y.; Duan, E.-p.; Xin, J.; Li, C. *Plasma Chem. Plasma Process.* **2012**, *32*, 1189−1201.

(8) Huiskamp, T.; Hoeben, W. F. L. M.; Beckers, F. J. C. M.; van Heesch, E. J. M.; Pemen, A. J. M. *J. Phys. D: Appl. Phys.* **2017**, *50*, No. 405201.

(9) Khacef, A.; Cormier, J. M.; Pouvesle, J. M. *J. Phys. D: Appl. Phys.* **2002**, *35*, 1491−1498.

(10) Khacef, A.; Cormier, J. M.; Pouvesle, J. M. *J. Adv. Oxid. Technol.* **2005**, *8*, No. 150.

(11) Shimizu, K.; Kinoshita, K.; Yanagihara, K.; Rajanikanth, B. S.; Katsura, S.; Mizuno, A. *IEEE Trans. Ind. Appl.* **1997**, *33*, 1373−1380.

(12) Shimomura, N.; Fukawa, F.; Akiyama, H. In *Treatment of Nitrogen Oxides Using Nanosecond Width Pulsed Power*, Conference Record of the 2006 Twenty-Seventh International Power Modulator Symposium, May 14−18, 2006; pp 321−324.

(13) Shimomura, N.; Nakano, K.; Nakajima, H.; Kageyama, T.; Teranishi, K.; Fukawa, F.; Akiyama, H. *IEEE Trans. Dielectr. Electr. Insul.* **2011**, *18*, 1274−1280.

(14) Morimoto, M.; Arai, R.; Omatsu, K.; Teranishi, K.; Shimomura, N. *IEEE Trans. Plasma Sci.* **2016**, *44*, 2874−2879.

(15) Omatsu, K.; Arai, M.; Morimoto, M.; Shimomura, N.; Teranishi, K. In *Observation of Discharges in NO_x Treatment Reactor Using Nanosecond Pulsed Powers and the Reactor Improvement*, 2016 IEEE International Power Modulator and High Voltage Conference (IPMHVC), July 6−9, 2016; pp 382−385.

(16) Vinh, T. Q.; Watanabe, S.; Furuhata, T.; Arai, M. *J. Mech. Sci. Technol.* **2012**, *26*, 1921−1928.

(17) Namihira, T.; Wang, D.; Akiyama, H. *Acta Phys. Pol., A* **2009**, *115*, 953−955.

(18) Matsumoto, T.; Wang, D. Y.; Namihira, T.; Akiyama, H. *IEEE Trans. Plasma Sci.* **2010**, *38*, 2639−2643.

(19) Schroeder, C.; Schroeder, W.; Yang, S.; Nystrom, A.; Cai, Z.; Subramanian, S.; Li, S.; Gundersen, M. A.; Cronin, S. B. *Fuel Process. Technol.* **2020**, *208*, No. 10652.

(20) Fleischmann, M.; Hendra, P. J.; McQuillan, A. J. *Chem. Phys. Lett.* **1974**, *26*, 163−166.
(21) Jeanmaire, D. L.; Van Duyne, R. P. *J. Electroanal. Chem. Interfacial Electrochem.* **1977**, *84*, 1−20.
(22) Albrecht, M. G.; Creighton, J. A. *J. Am. Chem. Soc.* **1977**, *99*, 5215−5217.
(23) Shi, H.; Cai, Z.; Patrow, J.; Zhao, B.; Wang, Y.; Wang, Y.; Benderskii, A.; Dawlaty, J.; Cronin, S. B. *ACS Appl. Mater. Interfaces* **2018**, *10*, 33678−33683.
(24) Shi, H.; Pekarek, R. T.; Chen, R.; Zhang, B.; Wang, Y.; Aravind, I.; Cai, Z.; Jensen, L.; Neale, N. R.; Cronin, S. B. *J. Phys. Chem. C* **2020**, *124*, 17000−17005.
(25) Chen, R.; Jensen, L. *J. Chem. Phys.* **2020**, *152*, No. 024126.
(26) Jensen, L.; Aikens, C. M.; Schatz, G. C. *Chem. Soc. Rev.* **2008**, *37*, 1061−1073.
(27) Zhao, B.; Aravind, I.; Yang, S.; Wang, Y.; Li, R.; Cronin, S. B. *ACS Appl. Nano Mater.* **2020**, *3*, 12388−12393.
(28) Zhao, B.; Aravind, I.; Yang, S.; Wang, Y.; Li, R.; Zhang, B.; Wang, Y.; Dawlaty, J. M.; Cronin, S. B. *J. Phys. Chem. C* **2021**, *125*, 6800−6804.
(29) Zhao, B.; Aravind, I.; Yang, S.; Cai, Z.; Wang, Y.; Li, R.; Subramanian, S.; Ford, P.; Singleton, D. R.; Gundersen, M. A.; Cronin, S. B. *J. Phys. Chem. C* **2020**, *124*, 7487−7491.
(30) Matsuta, H.; Hirokawa, K. *Appl. Spectrosc.* **1989**, *43*, 239−245.
(31) Kurokawa, Y.; Imai, Y.; Sasaki, Y.; Maeda, T. *Anal. Biochem.* **1993**, *209*, 247−250.
(32) Kim, S.; Kim, D.-H.; Park, S.-G. *Analyst* **2018**, *143*, 3006−3010.
(33) Von Raben, K. U.; Dorain, P. B.; Chen, T. T.; Chang, R. K. *Chem. Phys. Lett.* **1983**, *95*, 269−273.
(34) Matsuta, H.; Hirokawa, K. *Surf. Sci.* **1986**, *172*, L555−L560.

https://doi.org/10.1021/acs.analchem.0c05413
Anal. Chem. XXXX, XXX, XXX−XXX